
EFFICIENT CLASSIFICATION OF HISTOPATHOLOGY IMAGES USING HIGHLY IMBALANCED DATA

Mohammad Iqbal Nouyed
West Virginia University
Morgantown WV 26506, USA
monouyed@mix.wvu.edu

Mary-Anne Hartley
Yale University School of Medicine
New Haven, CT 06510, USA
mary-anne.hartley@yale.edu

Gianfranco Doretto, Donald A. Adjeroh
West Virginia University
Morgantown WV 26506, USA
{gianfranco.doretto, donald.adjeroh}@mail.wvu.edu

ABSTRACT

This work addresses how to efficiently classify challenging histopathology images, such as gigapixel whole-slide images for cancer diagnostics with image-level annotation. We use images with annotated tumor regions to identify a set of tumor patches and a set of benign patches in a cancerous slide. Due to the variable nature of region of interest the tumor positive regions may refer to an extreme minority of the pixels. This creates an important problem during patch-level classification, where the majority of patches from an image labeled as 'cancerous' are actually tumor-free. This problem is different from semantic segmentation which associates a label to every pixel in an image, because after patch extraction we are only dealing with patch-level labels. Most existing approaches address the data imbalance issue by mitigating the data shortage in minority classes in order to prevent the model from being dominated by the majority classes. These methods include data re-sampling, loss re-weighting, margin modification, and data augmentation. In this work, we mitigate the patch-level class imbalance problem by taking a divide-and-conquer approach. First, we partition the data into sub-groups, and define three separate classification sub-problems based on these data partitions. Then, using an information-theoretic cluster-based sampling of deep image patch features, we sample discriminative patches from the sub-groups. Using these sampled patches, we build corresponding deep models to solve the new classification sub-problems. Finally, we integrate information learned from the respective models to make a final decision on the patches. Our result shows that the proposed approach can perform competitively using a very low percentage of the available patches in a given whole-slide image.

Keywords histopathology image · data imbalance · patch classification

1 Introduction

Whole-slide images (WSIs) are a rich source of information in digital histology, where tissue sections are scanned at gigapixel scale at various microscopic magnification levels [1, 2]. However, the size and number of these images pose challenges for machine learning models. Firstly, the gigapixel resolution creates memory constraints necessitating input fragmentation. Secondly, annotations of the tumor regions may constitute a very tiny portion of the entire WSI which can create a large class imbalance in the training data. In recent years, deep models like CNNs and Transformer-based weakly supervised learning methods such as multiple-instance learning (MIL) have shown promising results in gigapixel whole slide image classification with varied sizes. In this approach, WSIs are divided into small image tiles or patches and then aggregated in later stages to make prediction using a classifier [3, 4, 5]. MIL treats each WSI as a bag containing multiple instances. If any instance of a WSI is disease-positive then the whole bag (WSI) is labeled as disease-positive. An aggregator classifier is used on the instance-level predictions to get the final image level prediction.

Real-world datasets often display long-tailed or imbalanced class distributions [6, 7, 8, 9]. Common approaches to handling data imbalance work by mitigating the data shortage in minority class by data augmentation [10, 11, 12], margin modification [13], loss re-weighting [14, 15, 16], and data re-sampling [17, 18, 19, 20]. Though these methods have performed well on imbalanced natural image data, they may not be as effective for WSIs. This is because, in the MIL classifier, the WSI is represented as a bag of image tiles of variable sizes [21]. However, since the area of the image that actually contains tumor in a WSI can be very small, it means that a majority of tiles in an image weakly labeled 'cancerous' actually do not contain tumor, effectively mislabeling (>80%) of the tiles[22].

To address these challenges, we propose a patch-level classification method that utilizes cluster-based sampling strategy to solve the imbalance problem between tumor and benign class patches and also provides an efficient histopathology image classification framework for resource-constrained scenarios. The main contributions of this work are as follows:

- A group based training approach where we divide the data into three specific sets which help us to decompose the original problem into three sub-problems. Each sub-problem focuses on discriminating between specific binary classification problems and, when combined, solves the original classification challenge effectively.
- A z-score-based stratified sampling on clustered image patches of the three focus data groups, which allows us to sample most of the patch texture variety by selecting patches from all the distance-based intervals from cluster centroid.
- A learning based information integration from the three sub-problems to obtain the final image level predictions.

2 Related Work

2.1 Multiple Instance Learning (MIL) for WSI Classification

A typical MIL method for WSI classification consists of two stages. First, features are extracted from each instance, and then these instance features are aggregated to obtain a bag-level feature. Then, an image (bag) level classifier is trained using the bag-level features and their corresponding labels. Lin et al. [23] proposed a model-agnostic framework called CIMIL to improve existing MIL models by using a counterfactual inference-based subbag evaluation method and a hierarchical instance searching strategy to help search reliable instances and obtain their accurate pseudo-labels. Qu et al. [24] proposed a feature distribution-guided MIL framework called DGMIL, for both WSI classification and positive patch localization. Shi et al. [25] proposed a loss based attention mechanism, which simultaneously learns instance weights and predictions, and bag predictions for deep MIL. Qu et al. [26] proposed an end-to-end weakly supervised knowledge distillation framework called WENO for WSI classification. Li et al. [5] proposed a deep MIL model, called DSMIL, which jointly learns a patch (instance) and an image (bag) classifier, using a two-stream architecture. Zhang et al. [4] proposed to virtually enlarge the number of bags by introducing the concept of pseudobags, on which a double-tier MIL framework, called DFTD-MIL, is built to effectively use the intrinsic feature. Kong et al. [22] presented an end-to-end CNN model called the Zoom-In network that uses hierarchical attention sampling to classify gigapixel pathology images with minority-pixel cancer metastases from the CAMELYON16 dataset. Sharma et al. [27] proposed an end-to-end framework named Cluster-to-Conquer (C2C) that clusters the patches from a WSI into k -groups, samples k' patches from each group for training, and uses an adaptive attention mechanism for slide-level prediction. Campanella et al. [28] presented a deep learning system based on multiple instances of learning that uses only the diagnoses reported as labels for training, thereby avoiding expensive and time-consuming pixel-wise manual annotations. Lu et al. [29] reported an interpretable weakly supervised deep-learning method called CLAM that uses attention-based learning to identify sub-regions of high diagnostic value to accurately classify whole slide images. Nouyed et al [30] addressed the challenge of high resolution image classification using a discriminative patch selection approach where they embed their patch selection approach inside a novel classification framework which can support the use of different off-the-shelf deep models.

While all the works mentioned above focus on solving the problem of patch-level label corruption from weakly assigned labels at the image level, they do not address the frequent issue of patch class imbalance, where the region of interest (ROI) that defines the label occupies a super minority of the image pixel space. Pawlowski et al. [31] investigated the performance of CNNs for minority-pixel image classification tasks and their results show that by using a training dataset limited in size, CNNs fail to generalize well because of the low ROI-to-image ratio. Usually, the object associated with the label occupies a dominant portion of the image. However, in histopathology image classification such as gigapixel whole-slide image classification, there could be datasets where only a very tiny fraction of the image informs the positive label.

2.2 Long-tailed histopathology image classification

Long-tailed classification is a well-known research topic in machine learning where the objective is to solve the data imbalance problem [32, 33]. Under-sampling [34, 18, 20] and over-sampling [35, 36] are common solutions with known trade-offs between bias and accuracy. While over-sampling can lead to overfitting of the minority class [19], under-sampling has the potential of information loss about the majority class [18]. We can also apply data augmentation to amplify the minority classes [11, 12]. Another category of data balancing is called loss re-weighting, in which the loss function is modified to increase weight on the minority class samples and decrease weight on the majority class samples [37, 38, 16]. But research has shown that loss re-weighting can be ineffective when the datasets are separable [39].

3 Method

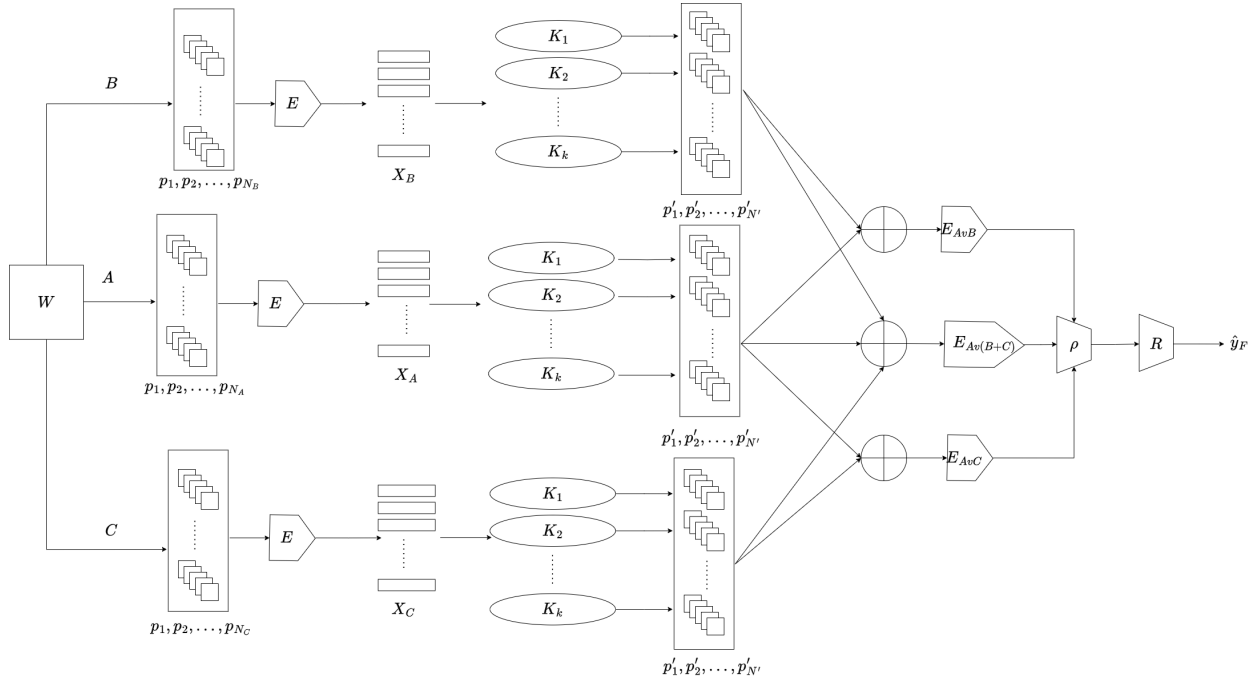


Figure 1: Overview of the proposed framework. At the first stage, all patches of WSIs are extracted using a pre-trained model E . Then based on available annotation train set data is categorized into 3 data sub-sets. Feature set X_A, X_B, X_C are extracted from each corresponding set. On each set clustering K is performed and then z-score based cluster sampling strategy is applied. Then 3 different models E_{AvB}, E_{AvC} and $E_{Av(B+C)}$ are fine-tuned using the sampled patches $\{p'_1, p'_2, \dots, p'_N\}$ to train the binary classification models $E_{AvB}, E_{AvC}, E_{Av(B+C)}$. From these, the feature or aggregation information is passed to the aggregation function $\rho(\cdot)$ for patch-level aggregation. And, these aggregated information is used for final patch-level decision fusion using the final R classifier.

In MIL, a group of training samples is considered as a bag containing multiple instances. Each bag has a bag label that is positive if the bag contains at least one positive instance and negative if it contains no positive instance. The instance-level labels are unknown. In the case of binary classification, let $B = \{(x_1, y_1), \dots, (x_n, y_n)\}$ be a bag where $x_i \in \mathcal{X}$ are instances with labels $y_i \in \{0, 1\}$, the label of B is given by

$$c(B) = \begin{cases} 0, & \text{iff } \sum y_i = 0 \\ 1, & \text{otherwise} \end{cases} \quad (1)$$

First, the image is split into $N \times N$ instances of equal size. We consider the instances from the same image as in the same bag. The main components of our method can be divided into four parts, (1) A divide-and-conquer approach is taken by splitting training data into 3 patch sets using pseudo-labeling and ROI; (2) partitioning of the cancer classification

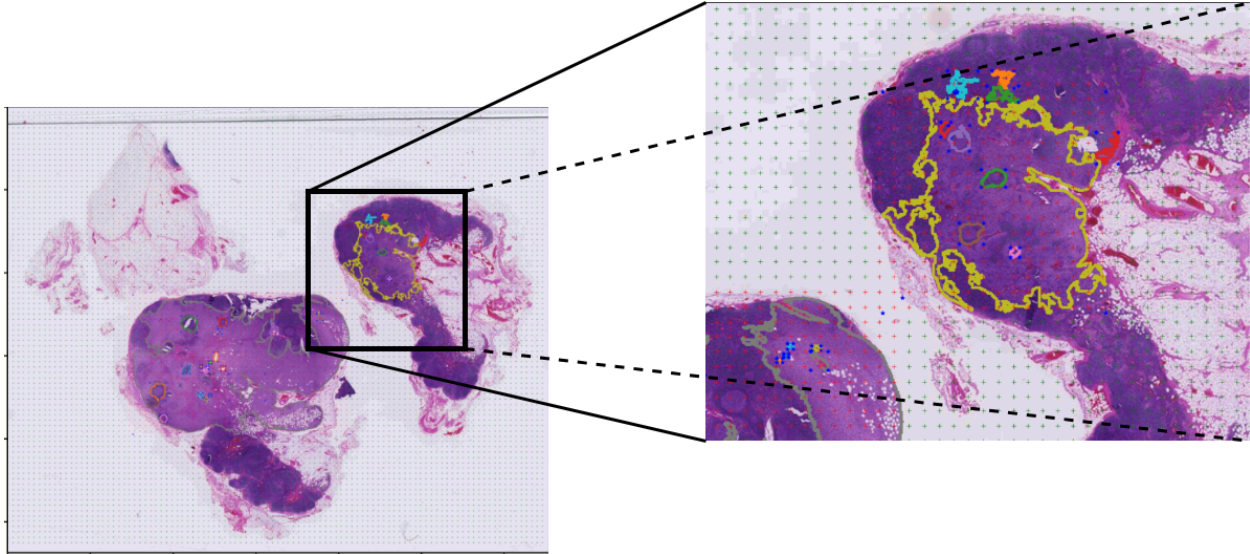


Figure 2: Sample WSI, with annotation. Zoomed in section includes annotated regions in different colors, also, the '+' signs indicates the patch 256×256 boundaries extracted.

problem into smaller sub-problems based on tumor annotation and source of tissue sample; and (3) Integration of the patch level results using patch level pooling at the feature and prediction levels, followed by activation function and dimensionality reduction (if needed), (4) A threshold percentage of tumor patch per WSI is used to determine the final patch level prediction. Figure 1 provides an overview of the proposed framework, while Figure 2 shows a sample WSI with annotated tumor region

3.1 Partition-based approach to WSI analysis

Based on the annotation provided in the dataset, we categorize the patches into three different types: 1) Set of tumor patches, denoted as A , so A can be defined as $A = \{(x, y_p) | y_p = 1, x \in W, y_w = 1\}$, where x is an image patch, y_p is patch label, W is an image, and y_w is image label; 2) Set of benign patches that belong to WSIs labeled as cancerous, denoted as set B , so $B = \{(x, y_p) | y_p = 0, x \in W, y_w = 1\}$; (Note that, set B does not indicate a misclassification, a doctor's misdiagnosis, nor a system's misdetection. It is simply the set of patches that are extracted outside the annotated tumor regions of the WSI.); and 3) Set of benign patches that belong to WSIs labeled as benign, denoted as set C , so $C = \{(x, y_p) | y_p = 0, x \in W, y_w = 0\}$. The assumption is that the benign patches belonging to a cancerous WSI may contain additional information that can help the model learn to better discriminate between tumor and tumor-free patches. Based on these three data partitions, we can now decompose the original problem into three different binary classification sub-problems: 1) A versus B , 2) A versus C and 3) A versus $(B+C)$. We then train three different classification models of the same architecture for each of the patch-level classification sub-problems.

3.2 Information theoretic cluster-based sampling

Algorithmus 1 Information-theoretic cluster-based patch sampling algorithm

Require: $X, K, |A|$
Ensure: P

```

1: for  $K_1, K_2, \dots, K_k$  do
2:   for  $x \in X$  do
3:      $d \leftarrow JSD(K_k, x); D(k) \leftarrow D(k) \cup d$ 
4:   end for
5:    $D_\sigma(k) \leftarrow \sigma(D(k)); D_\mu(k) \leftarrow \mu(D(k))$ 
6:   for  $d \in D(k)$  do
7:      $z \leftarrow \frac{d - D_\mu(k)}{D_\sigma(k)}; Z(k) \leftarrow Z(k) \cup z$ 
8:   end for
9: end for
10: for  $K_1, K_2, \dots, K_k$  do
11:    $S_T = |A| * ||D_\mu(k)||$ 
12:   for  $x \in X$  do
13:      $d \leftarrow JSD(K_k, x); z \leftarrow \frac{d - D_\mu(k)}{D_\sigma(k)}; i \leftarrow GetInterval(z); X'(i) \leftarrow x$ 
14:   end for
15:    $s_i = \lfloor S_T / |X'| \rfloor$ 
16:   while true do
17:     for  $i \in X'$  do
18:        $\rho \leftarrow RandomSample(X'(i)); P \leftarrow P \cup \rho; S_T \leftarrow S_T - |\rho|$ 
19:     end for
20:      $Update(X'); s_i = \lfloor S_T / |X'| \rfloor$ 
21:     if  $S_T \leq 0$  or  $s_i \leq 0$  then
22:       break
23:     end if
24:   end while
25: end for

```

Because of the partition of the patch sets, we now have a clearer understanding of the class imbalance between the benign and tumor patches. Typically for a dataset $|A| \ll |B|$ and $A \ll |C|$. For this reason, we apply a sampling approach to reduce the class imbalance among set A , B and, C . First using a pre-trained model, we extract features from all patches. Let $X \leftarrow f(B, \theta)$ or $X \leftarrow f(C, \theta)$, where $f(\cdot, \theta)$ is a feature extractor using the trained parameters θ . We use a parametric clustering method to cluster each of the sets into k different clusters, such that, K_k is the k -th cluster centroid. Given a set of patch features (x_1, x_2, \dots, x_n) , where each patch has been converted to a d -dimensional real vector, parametric clustering such as k-means aims to partition the n patches into k clusters ($k \leq n$) sets $\mathbf{S} = \{S_1, S_2, \dots, S_k\}$ so as to iteratively minimize the within-cluster sum of square errors to reach the local minima or optimum. The objective can be defined as :

$$\underset{S}{\operatorname{argmin}} \sum_{i=1}^k \sum_{\mathbf{x} \in S_i} \|\mathbf{x} - \mu_i\|^2 \quad (2)$$

where, μ_i is the mean or centroid of the points in S_i , $\mu_i = \frac{1}{|S_i|} \sum_{\mathbf{x} \in S_i} \mathbf{x}$. We use these k clusters to perform a systematic sampling on the patches such that we can create balanced sets that is not dominated by the minority class. Algorithm 1 shows our procedure for this information-theoretic cluster-based sampling to generating balanced patch sets. Based on the available tumor patches, we sample equal number of patches from each of the k cluster sets, if B' and C' are the new sampled sets such that $B' \subset B$ and $C' \subset C$ then $|B'| = |A|$, $|C'| = |A|$. Denote $P = B'$ or C' . During clustering we take a stratified random sampling approach based on the Euclidean distance from the cluster centroid in order to maximize the intra cluster variance among the clusters by sampling in such a way that P contains samples from all z-score intervals $X'(i)$. For a given patch in a cluster, we represent its computed features as a probability distribution. Similarly with the cluster centroid. We then use an information-theoretic divergence measure, namely the Jensen-Shannon divergence (JSD), to evaluate the dispersion between the patch, and its cluster centroid. For two probability distributions p_1 and p_2 , the Jensen-Shannon divergence[40] is given by:

$$JSD(p_1, p_2) = \frac{1}{2}D(p_1||q) + \frac{1}{2}D(p_2||q) \quad (3)$$

where $q = \frac{1}{2}(p_1 + p_2)$, and $D(p_1||q)$ is the Kullback-Leibler (KL) divergence [40] between two distributions, given by:

$$D(p_1||q) = \sum_{c=1}^{|C|} p_1(c) \log \left(\frac{p_1(c)}{q(c)} \right) \quad (4)$$

where C is the number of distinct intervals used in the representation. For each cluster we divide the distribution into intervals based on the z-scores. Then for each patch we calculate the z-score of its dispersion from the centroid $z \leftarrow \frac{d-D_\mu(k)}{D_\sigma(k)}$. Based on this, we make sure we uniformly sample from each z-score interval as much as possible so that we can have representation of all possible patch texture variances as much as possible from each cluster, while keeping the total sample size within S_T where $S_T = |A| * ||D_\mu(k)||$. Essentially, S_T is the value we get by multiplying the expected total size of the sampled set with normalized mean of all centroid dispersions (or centroid distances). A pseudo-code based description is provided in Algorithm 1.

3.3 Instance level learning

The instance-level models encode patches to a d -dimensional embedding, $f(\mathbf{x}, \theta) : \mathbf{x} \rightarrow \mathbf{h}$ where θ is the set of training parameters. During the training, we use the cross entropy loss on the instance-level labels and prediction of the selected instance to update the classifier's parameters. The loss function for the classifier is define as follows:

$$L = - \sum_j y_j \log \hat{y}_j + (1 - y_j) \log(1 - \hat{y}_j), \quad (5)$$

where y_j is the instance-level label. Using the partitioned datasets A, B and C we train three different binary classification models, that learns to discriminate between A vs. B, A vs. C, and A vs. (B+C), respectively. The objective here is to divide the problem space into sub-problems that discriminate between tumor and benign regions within same tissue image (AvB); between tumor and benign regions of other tissue images (AvC), and tumor and benign regions of both same and other tissue image (Av(B+C)). The assumption is that the aggregated feature representations obtained from these expert binary classification models will be more informative for the final prediction. See Figure 1.

3.4 Integrating information from Problem Decompositions

We investigate information integration from the sub-problems in 5 different ways: (M0) Majority vote based on the fine-tuned deep model predictions: Let, $\hat{Y}_{AvB} = \{\hat{y}_i | f_{AvB}^\theta(x_i, y_i) \rightarrow \hat{y}_i\}$, $\hat{Y}_{AvC} = \{\hat{y}_i | f_{AvC}^\theta(x_i, y_i) \rightarrow \hat{y}_i\}$ and $\hat{Y}_{Av(B+C)} = \{\hat{y}_i | f_{Av(B+C)}^\theta(x_i, y_i) \rightarrow \hat{y}_i\}$, are the set of instance-level predictions obtained from models trained on the AvB, AvC, and Av(B+C) datasets. Here f_{AvB} , f_{AvC} , $f_{Av(B+C)}$ are the binary classification models trained on some parameters θ , and \hat{y}_i is the predicted label of the i -th instance. Then we perform a simple majority vote count based on the number of positive predictions to obtain \hat{y}_F , the fused label; (M1) Learning-based fusion using Softmax: Let, $S_{AvB} = \{\sigma_i | \mathcal{S}(f_{AvB}^\theta(x_i, y_i)) \rightarrow \sigma_i\}$, $S_{AvC} = \{\sigma_i | \mathcal{S}(f_{AvC}^\theta(x_i, y_i)) \rightarrow \sigma_i\}$ and $S_{Av(B+C)} = \{\sigma_i | \mathcal{S}(f_{Av(B+C)}^\theta(x_i, y_i)) \rightarrow \sigma_i\}$ be a set of instance-level probability distributions, where $\mathcal{S}(\cdot)$ is the softmax function. These instance level probability distributions are concatenated to x and passed to a classifier; (M2) learning-based fusion using feature concatenation followed by dimensionality reduction: Let, $X_{AvB} = \{x_i | E_{AvB}^\theta(x_i) \rightarrow x_i\}$, $X_{AvC} = \{x_i | E_{AvC}^\theta(x_i) \rightarrow x_i\}$ and $X_{Av(B+C)} = \{x_i | E_{Av(B+C)}^\theta(x_i) \rightarrow x_i\}$, be the set of feature representations obtained from the trained feature encoders E_{AvB}^θ , E_{AvC}^θ , $E_{Av(B+C)}^\theta$. These features are concatenated to x and then passed to a dimensionality reduction function $PCA(\cdot)$ followed by a classifier; (M3) Learning-based fusion by applying dimensionality reduction on individual features and then concatenation. Similar to (M2), but here first $PCA(\cdot)$ is applied on individual feature representation and then the reduced features are concatenated; and (M4) Instance level pooling of learned features followed by activation functions and then applying a classifier. Average pooling method on the instance level features is applied to obtain an aggregated patch level representation. This aggregated representation is then passed to GeLU ($G(z)$) function followed by a classifier, where $G(z)$ is defined as follows.

$$G(z) = 0.5x(1 + \tanh[\sqrt{2/\pi}(x + 0.044715x^3)]) \quad (6)$$

Algorithm 2 shows our proposed procedures for integrating information obtained from solving the three sub-problems.

Algorithmus 2 Information integration from the problem decomposition

Require: $X_{AvB}, X_{AvC}, X_{Av(B+C)}, \hat{Y}_{AvB}, \hat{Y}_{AvC}, \hat{Y}_{Av(B+C)}, S_{AvB}, S_{AvC}, S_{Av(B+C)}, Y, m$
Ensure: \hat{y}_F

- 1: **if** $m = 0$ **then**
- 2: **for** $\hat{y}_1 \in \hat{Y}_{AvB}, \hat{y}_2 \in \hat{Y}_{AvC}, \hat{y}_3 \in \hat{Y}_{Av(B+C)}$ **do**
- 3: **if** $\hat{y}_1 + \hat{y}_2 + \hat{y}_3 \geq 2$ **then** return 1 **else if** return 0 **end if**
- 4: **end for**
- 5: **else if** $m = 1$ **then**
- 6: **for** $\sigma_1 \in S_{AvB}, \sigma_2 \in S_{AvC}, \sigma_3 \in S_{Av(B+C)}, y \in Y$ **do**
- 7: $x \leftarrow [\sigma_1; \sigma_2; \sigma_3]; \hat{y}_F \leftarrow \text{RandomForest}(x, y);$ return \hat{y}_F
- 8: **end for**
- 9: **else if** $m = 2$ **then**
- 10: **for** $x_1 \in X_{AvB}, x_2 \in X_{AvC}, x_3 \in X_{Av(B+C)}, y \in Y$ **do**
- 11: $x \leftarrow [x_1; x_2; x_3]; x' \leftarrow \text{PCA}(x); \hat{y}_F \leftarrow \text{RandomForest}(x', y);$ return \hat{y}_F
- 12: **end for**
- 13: **else if** $m = 3$ **then**
- 14: **for** $x_1 \in X_{AvB}, x_2 \in X_{AvC}, x_3 \in X_{Av(B+C)}, y \in Y$ **do**
- 15: $x'_1 \leftarrow \text{PCA}(x_1), x'_2 \leftarrow \text{PCA}(x_2); x'_3 \leftarrow \text{PCA}(x_3)$
- 16: $x' \leftarrow [x'_1; x'_2; x'_3]; \hat{y}_F \leftarrow \text{RandomForest}(x', y);$ return \hat{y}_F
- 17: **end for**
- 18: **else if** $m = 4$ **then**
- 19: **for** $x_1 \in X_{AvB}, x_2 \in X_{AvC}, x_3 \in X_{Av(B+C)}, y \in Y$ **do**
- 20: $x'_p \leftarrow \text{AvgPool}([x'_1; x'_2; x'_3]); x' \leftarrow \text{GeLU}(x'_p)$
- 21: $\hat{y}_F \leftarrow \text{RandomForest}(x', y);$ return \hat{y}_F
- 22: **end for**
- 23: **end if**

4 Experiments and Results

4.1 Database

We use the publicly available CAMELYON16 dataset for breast cancer metastasis detection. It has a total of 399 WSIs, with 270 WSIs in training and 129 WSIs in test set. Out of the 270 training images, 111 are tumor WSIs, whose tumor annotation is also provided. For our work, patches of size 256×256 at $10\times$ magnification were extracted. Table 1 provides both slide-level and patch-level database details. Figure 2 shows a sample WSI with tumor annotation.

Table 1: CAMELYON16 dataset details with info on 256×256 size patches extracted at $10\times$ magnification level.

		Train	Test
Image level (WSI)	Total number	270	129
	Positives (number, %)	111 (41%)	49 (31%)
	Negatives (number, %)	159 (59%)	80 (62%)
	Avg. area of ROI (pixels, %)	444,770 (0.003%)	653,670 (0.005%)
	Max area of ROI (pixels, %)	91,418,800 (0.8%)	332,954,015 (2.8%)
	Min area of ROI (pixels, %)	10 (0.000%)	0 (0.000%)
Patch level	Total number	4,612,746	2,026,538
	Positives (number, %)	38,052 (0.8%)	31,536 (1.56%)
	Negatives (number, %)	4,574,694 (99%)	1,995,131 (98%)
Patches/Image (PPI)	Average	17083	15710
	Max	22,787	20,906
	Min	1,461	3,093

4.2 Architecture and hardware

For all models, we used ResNet-18 [41] with a $l = 512$ feature representation which was then clustered using k-means with l_2 -normalization. The model was implemented with PyTorch and trained on a single RTX1080 GPU. The models are trained using an SGD optimizer with a batch size of 512 and a learning rate of $1e - 4$ for 10 epochs.

4.3 Patch labeling

To partition the patches into groups (A, B, and C), first we find the bounding box around the tumor polygons provided by the CAMELYON16 dataset. After that, for each patch of a WSI, we detect if there is any overlap between the polygon bounding box and the patch coordinates, if there is an overlap we calculate the area of overlapping rectangles using the following formula:

$$(\min(x_2, p_2) - \max(x_1, p_1)) * (\min(y_2, q_2) - \max(y_1, q_1)) \quad (7)$$

where $(x_1, y_1), (x_2, y_2)$ are the polygon bounding box, and $(p_1, q_1), (p_2, q_2)$ are the patch coordinates. We use an overlap threshold to decide whether to assign the patch of a tumor positive WSI in A set, or in the B set, and, if the WSI is tumor negative we put the patches in C set.

Table 2: Distribution of patches after partitioning into the 3 groups and after applying the clustering based sampling algorithm to create balanced sets.

		A	B	C	Total
Unbalanced data	Train	30,442	1,505,762	2,153,994	3,690,198
	Val	7,610	376,440	538,498	922,548
	Total	38,052	1,882,202	2,692,492	4,612,746
Balanced data	Train (number, %)	30,442 (100%)	30,440 (2%)	30,440 (1.4%)	91,322 (2.4%)
	Val (number, %)	7,610 (100%)	7,609 (2%)	7,609 (1.4%)	22,828 (2.4%)
	Total (number, %)	38,052 (100%)	38,049 (2%)	38,049 (1.4%)	114,150 (2.4%)

4.4 Patch sampling

We apply a K-means clustering algorithm, with $k = 10$, on the pre-trained ResNet18 [41] features of the unbalanced training set. Now to sample from the B set and C set patches, equal to the size of A set, we use the Euclidean distance from centroid feature to patch feature. The z-score intervals span from -3 to 15, and patches are sampled from within these intervals. Table 2 provides the details on both unbalanced and balanced training and validation datasets. We can observe that for the training and validation set we tried to keep the A set patches as much as possible so that we don't lose any information regarding tumor presence in the slides. The contributions of the cluster-based sampling strategy or the z-score based sampling strategy were visible, when we compared its performance with just random sampling once the sub-groups of patches are formed. We have found due to the Gaussian nature of the random sampling algorithm most of the patches were similar and does not represent all the variable texture patches within the centroid. This motivated us to take the z-score based sampling approach so that we can properly sample representations from all ranges of variability within a cluster.

4.5 Efficiency

From Table 2, we can observe that we have used 100% of all A set patches for the training and validation set construction, but reduced the majority classes (namely, class B and class C) down to 2% and 1.4% of the original dataset, respectively, in order to match with the minority class. Since during training time these patches are processed sequentially, the time that can be saved can be estimated as $\mathcal{O}(B/U)$, where B is the total size of the balanced data, and U is the total size of the unbalanced data. Thus, from the table, the proposed method will run about 50 times faster than working without the proposed sampling approach. Note that, we are estimating the efficiency gain based on the presence of the balancing step in the proposed framework. We also observe that, speed of convergence is another aspect of measuring the efficiency of the balancing approach which can further establish the efficacy of the balancing step.

Table 3: Cross validation result for the 3 models.

	AvB	AvC	Av(B+C)
	Top-1 Acc.	Top-1 Acc.	Top-1 Acc.
Avg.±Std.	0.894 ± 0.023	0.902 ± 0.022	0.897 ± 0.011

4.6 Evaluation

Using the balanced A, B and C sets, we create 5-fold cross validation sets (80-20 partition). We evaluated performances of the models trained on AvB, AvC and Av(B+C) models, individually and also using feature aggregated decision fusion approaches. Table 3 shows the individual cross-validation performance of the 3 binary classification models on the

Table 4: Patch-level classification performance using the proposed models for information integrating from the problem decompositions.

Methods	Accuracy	AUC	Precision	Recall	F1-score
M0	0.833 ± 0.001	0.833 ± 0.001	0.764 ± 0.001	0.963 ± 0.001	0.852 ± 0.001
M1	0.980 ± 0.001	0.980 ± 0.001	0.964 ± 0.002	0.997 ± 0.001	0.980 ± 0.001
M2	0.989 ± 0.000	0.989 ± 0.001	0.978 ± 0.001	0.999 ± 0.000	0.988 ± 0.001
M3	0.988 ± 0.001	0.989 ± 0.001	0.978 ± 0.001	0.999 ± 0.000	0.988 ± 0.000
M4	0.987 ± 0.001	0.987 ± 0.004	0.975 ± 0.001	0.999 ± 0.000	0.987 ± 0.001

Table 5: Comparison of patch level classification performance with the state-of-the-art.

Methods	Accuracy	AUC
Loss-ABMIL [25]	0.803	0.848
CLAM-SB [29]	0.789	0.880
CLAM-MB [29]	0.799	0.878
DSMIL [5]	0.857	0.886
DSMIL+WENO [26]	0.901	0.930
DTFD-MIL [4]	0.870	0.893
DGMIL [24]	0.886	0.901
CLAM-SB+CIMIL [23]	0.921	0.943
M2 (Ours) ^a	0.989 ± 0	0.989 ± 0.001
M3 (Ours) ^a	0.988 ± 0.001	0.989 ± 0.001

^aReported accuracy and AUC is based on validation data.

balanced datasets. The average top-1 accuracies are 0.894 ± 0.023 , 0.902 ± 0.022 and 0.897 ± 0.011 showing strong patch level performance on the individual partitioned data sub-sets. This is using a relatively weak ResNet backbone architecture (ResNet-18). Table 4 shows the performance of different feature aggregation and decision fusion strategies using the combined folds from the 3 partitioned datasets. This makes the folds harder to predict because they include samples from all A, B, and C sets. Even after that we can see that feature concatenation followed by PCA and RF classification (*M2*) shows a strong performance of top-1 accuracy 0.989 along with high precision (0.978 ± 0.001), recall (0.999) and F1-score (0.988 ± 0.0005). The second best method utilizes PCA on deep features following by concatenation of dimensionality reduced features before classification (*M3*), has almost the same performance as *M2*. In fact, except for majority vote approach (M0), all 4 learning-based approaches show strong patch-level classification performance on the validation set. We believe this is indicative of the efficacy of our partitioning, sampling, and information integration from the three problem decompositions. Still the work has to show good performance on the test set also, which is much more challenging because we have to infer initial sub-divisions, followed by cluster sampling on an unseen data.

In Table 5 we provide comparative instance-level classification performance results with state-of-the-art methods. For our instance-level classification we used Area Under the Curve(AUC) and Top-1 accuracy as evaluation metrics to compare with other methods. We chose Loss-ABMIL [25], CLAM-SB [29], CLAM-MB [29], DSMIL+WENO [26], CLAM-SB+CIMIL [23], DSMIL [5], and DTFD-MIL [4]. ABMIL, CLAM, DSMIL models are equipped with specific mechanisms that provide patch prediction, DGMIL is specifically tailored for patch classification. WENO and CIMIL are frameworks for boosting existing MIL models. It can be seen that even with a significantly reduced dataset we were able to achieve the best instance-level performance both in terms of accuracy and AUC. We note that, with very high data imbalance, AUC is a much more effective performance metric than accuracy. However, since we handled the large class imbalance problem as part of our proposed approach, we believe it is appropriate to then include accuracy for performance measurement.

5 Conclusion

In this work, we propose a patch-level classification method that utilizes a group based training approach. By compartmentalizing training into sub-groups, we decompose the original classification problem into smaller classification sub-problems. We then develop models to solve each smaller sub-problem. Information from these models are later aggregated using feature and decision fusion approaches leading to a superior classification result. Furthermore, the method also incorporates a cluster-based sampling strategy to solve the significant data imbalance problem between positive and negative classes while maintaining slide-level representation of all WSIs. This allows our approach to

efficiently handle a large data source using limited computational resources. Strong patch-level performance in our cross-validation and data fusion experiments validates our claim. Future work should explore the transferable value of the patch level features for slide-level predictions and verify on test set data. More ablation studies is needed to further investigate the impact of various algorithmic parameters, e.g, the initial clustering, number of clusters, complexity of tumor patches, etc.

Acknowledgement

This work was supported in part by grants from the US National Science Foundation (Award #1920920 and #2125872).

References

- [1] Aleksandra Zuraw and Famke Aeffner. Whole-slide imaging, tissue image analysis, and artificial intelligence in veterinary pathology: An updated introduction and review. *Veterinary Pathology*, 59(1):6–25, 2022.
- [2] Neeta Kumar, Ruchika Gupta, and Sanjay Gupta. Whole slide imaging (wsi) in pathology: current perspectives and future directions. *Journal of Digital Imaging*, 33(4):1034–1040, 2020.
- [3] Zhuchen Shao, Hao Bian, Yang Chen, Yifeng Wang, Jian Zhang, Xiangyang Ji, and yongbing zhang. Transmil: Transformer based correlated multiple instance learning for whole slide image classification. In M. Ranzato, A. Beygelzimer, Y. Dauphin, P.S. Liang, and J. Wortman Vaughan, editors, *Advances in Neural Information Processing Systems*, volume 34, pages 2136–2147. Curran Associates, Inc., 2021.
- [4] Hongrun Zhang, Yanda Meng, Yitian Zhao, Yihong Qiao, Xiaoyun Yang, Sarah E. Coupland, and Yalin Zheng. DTFD-MIL: Double-tier feature distillation multiple instance learning for histopathology whole slide image classification. In *Proc. IEEE/CVF Conf. on Computer Vision and Pattern Recognition (CVPR)*, pages 18802–18812, June 2022.
- [5] Bin Li, Yin Li, and Kevin W. Eliceiri. Dual-stream multiple instance learning network for whole slide image classification with self-supervised contrastive learning. In *Proceedings of the IEEE/CVF Conference on Computer Vision and Pattern Recognition (CVPR)*, pages 14318–14328, June 2021.
- [6] Sara Fotouhi, Shahrokh Asadi, and Michael W. Kattan. A comprehensive data level analysis for cancer diagnosis on imbalanced data. *Journal of Biomedical Informatics*, 90:103089, 2019.
- [7] Qingfeng Wang, Xuehai Zhou, Chao Wang, Zhiqin Liu, Jun Huang, Ying Zhou, Changlong Li, Hang Zhuang, and Jie-Zhi Cheng. WGAN-based synthetic minority over-sampling technique: Improving semantic fine-grained classification for lung nodules in CT images. *IEEE Access*, 7:18450–18463, 2019.
- [8] S Deepak and PM Ameer. Brain tumor categorization from imbalanced mri dataset using weighted loss and deep feature fusion. *Neurocomputing*, 520:94–102, 2023.
- [9] Cong Cong, Yixing Yang, Sidong Liu, Maurice Pagnucco, and Yang Song. Imbalanced histopathology image classification using deep feature graph attention network. In *2022 IEEE 19th International Symposium on Biomedical Imaging (ISBI)*, pages 1–4, 2022.
- [10] Sankha Subhra Mullick, Shounak Datta, and Swagatam Das. Generative adversarial minority oversampling. In *Proc. IEEE/CVF Int’l Conf. on Computer Vision (ICCV)*, October 2019.
- [11] Jaehyung Kim, Jongheon Jeong, and Jinwoo Shin. M2m: Imbalanced classification via major-to-minor translation. In *Proceedings of the IEEE/CVF Conference on Computer Vision and Pattern Recognition (CVPR)*, June 2020.
- [12] Peng Chu, Xiao Bian, Shaopeng Liu, and Haibin Ling. Feature space augmentation for long-tailed data. In Andrea Vedaldi, Horst Bischof, Thomas Brox, and Jan-Michael Frahm, editors, *Computer Vision – ECCV 2020*, pages 694–710, Cham, 2020. Springer International Publishing.
- [13] Kaidi Cao, Colin Wei, Adrien Gaidon, Nikos Arechiga, and Tengyu Ma. Learning imbalanced datasets with label-distribution-aware margin loss. In H. Wallach, H. Larochelle, A. Beygelzimer, F. d’Alché-Buc, E. Fox, and R. Garnett, editors, *Advances in Neural Information Processing Systems*, volume 32. Curran Associates, Inc., 2019.
- [14] Jingru Tan, Changbao Wang, Buyu Li, Quanquan Li, Wanli Ouyang, Changqing Yin, and Junjie Yan. Equalization loss for long-tailed object recognition. In *Proceedings of the IEEE/CVF Conference on Computer Vision and Pattern Recognition (CVPR)*, June 2020.
- [15] Mengye Ren, Wenyuan Zeng, Bin Yang, and Raquel Urtasun. Learning to reweight examples for robust deep learning. In Jennifer Dy and Andreas Krause, editors, *Proceedings of the 35th International Conference on Machine Learning*, volume 80 of *Proceedings of Machine Learning Research*, pages 4334–4343. PMLR, 10–15 Jul 2018.

- [16] Yin Cui, Menglin Jia, Tsung-Yi Lin, Yang Song, and Serge Belongie. Class-balanced loss based on effective number of samples. In *Proceedings of the IEEE/CVF Conference on Computer Vision and Pattern Recognition (CVPR)*, June 2019.
- [17] Byron C. Wallace, Kevin Small, Carla E. Brodley, and Thomas A. Trikalinos. Class imbalance, redux. In *2011 IEEE 11th International Conference on Data Mining*, pages 754–763, 2011.
- [18] Ajinkya More. Survey of resampling techniques for improving classification performance in unbalanced datasets. *arXiv preprint arXiv:1608.06048*, 2016.
- [19] Nitesh V Chawla, Kevin W Bowyer, Lawrence O Hall, and W Philip Kegelmeyer. Smote: synthetic minority over-sampling technique. *Journal of Artificial Intelligence Research*, 16:321–357, 2002.
- [20] Mateusz Buda, Atsuto Maki, and Maciej A. Mazurowski. A systematic study of the class imbalance problem in convolutional neural networks. *Neural Networks*, 106:249–259, 2018.
- [21] Peng Wang, Kai Han, Xiu-Shen Wei, Lei Zhang, and Lei Wang. Contrastive learning based hybrid networks for long-tailed image classification. In *Proc. IEEE/CVF Conference on Computer Vision and Pattern Recognition (CVPR)*, pages 943–952, June 2021.
- [22] Fanjie Kong and Ricardo Henao. Efficient classification of very large images with tiny objects. In *Proceedings of the IEEE/CVF Conference on Computer Vision and Pattern Recognition (CVPR)*, pages 2384–2394, June 2022.
- [23] Weiping Lin, Zhenfeng Zhuang, Lequan Yu, and Liansheng Wang. Boosting multiple instance learning models for whole slide image classification: A model-agnostic framework based on counterfactual inference. *Proceedings of the AAAI Conference on Artificial Intelligence*, 38(4):3477–3485, Mar. 2024.
- [24] Linhao Qu, Xiaoyuan Luo, Shaolei Liu, Manning Wang, and Zhijian Song. Dgmil: Distribution guided multiple instance learning for whole slide image classification. In *Int’l Conf. on Medical Image Computing and Computer-Assisted Intervention*, pages 24–34. Springer, 2022.
- [25] Xiaoshuang Shi, Fuyong Xing, Yuanpu Xie, Zizhao Zhang, Lei Cui, and Lin Yang. Loss-based attention for deep multiple instance learning. In *Proceedings of the AAAI Conference on Artificial Intelligence*, volume 34, pages 5742–5749, 2020.
- [26] Linhao Qu, xiaoyuan luo, Manning Wang, and Zhijian Song. Bi-directional weakly supervised knowledge distillation for whole slide image classification. In S. Koyejo, S. Mohamed, A. Agarwal, D. Belgrave, K. Cho, and A. Oh, editors, *Advances in Neural Information Processing Systems*, volume 35, pages 15368–15381. Curran Associates, Inc., 2022.
- [27] Yash Sharma, Aman Shrivastava, Lubaina Ehsan, Christopher A. Moskaluk, Sana Syed, and Donald Brown. Cluster-to-conquer: A framework for end-to-end multi-instance learning for whole slide image classification. In Matthias Heinrich, Qi Dou, Marleen de Bruijne, Jan Lellmann, Alexander Schläfer, and Floris Ernst, editors, *Proceedings of the Fourth Conference on Medical Imaging with Deep Learning*, volume 143 of *Proceedings of Machine Learning Research*, pages 682–698. PMLR, 07–09 Jul 2021.
- [28] Gabriele Campanella, Matthew G Hanna, Luke Geneslaw, Allen Miraflor, Vitor Werneck Krauss Silva, Klaus J Busam, Edi Brogi, Victor E Reuter, David S Klimstra, and Thomas J Fuchs. Clinical-grade computational pathology using weakly supervised deep learning on whole slide images. *Nature Medicine*, 25(8):1301–1309, 2019.
- [29] Ming Y Lu, Drew FK Williamson, Tiffany Y Chen, Richard J Chen, Matteo Barbieri, and Faisal Mahmood. Data-efficient and weakly supervised computational pathology on whole-slide images. *Nature Biomedical Engineering*, 5(6):555–570, 2021.
- [30] Mohammad Iqbal Nouyed, Gianfranco Doretto, and Donald A. Adjeroh. Efficient classification of very high resolution histopathological images. In *2022 IEEE International Conference on Bioinformatics and Biomedicine (BIBM)*, pages 3114–3121, 2022.
- [31] Nick Pawlowski, Suvrat Bhooshan, Nicolas Ballas, Francesco Ciompi, Ben Glocker, and Michal Drozdal. Needles in haystacks: On classifying tiny objects in large images. *arXiv preprint arXiv:1908.06037*, 2020.
- [32] Miroslav Kubat, Stan Matwin, et al. Addressing the curse of imbalanced training sets: one-sided selection. In *ICML*, volume 97, page 179. Citeseer, 1997.
- [33] Grigoris Karakoulas and John Shawe-Taylor. Optimizing classifiers for imbalanced training sets. In M. Kearns, S. Solla, and D. Cohn, editors, *Advances in Neural Information Processing Systems*, volume 11. MIT Press, 1998.
- [34] Chris Drummond, Robert C Holte, et al. C4. 5, class imbalance, and cost sensitivity: why under-sampling beats over-sampling. In *Workshop on Learning from Imbalanced Datasets II*, volume 11, pages 1–8, 2003.

- [35] Nikolaos Sarafianos, Xiang Xu, and Ioannis A. Kakadiaris. Deep imbalanced attribute classification using visual attention aggregation. In *Proceedings of the European Conference on Computer Vision (ECCV)*, September 2018.
- [36] Li Shen, Zhouchen Lin, and Qingming Huang. Relay backpropagation for effective learning of deep convolutional neural networks. In Bastian Leibe, Jiri Matas, Nicu Sebe, and Max Welling, editors, *Computer Vision – ECCV 2016*, pages 467–482, Cham, 2016. Springer International Publishing.
- [37] Salman H. Khan, Munawar Hayat, Mohammed Bennamoun, Ferdous A. Sohel, and Roberto Togneri. Cost-sensitive learning of deep feature representations from imbalanced data. *IEEE Transactions on Neural Networks and Learning Systems*, 29(8):3573–3587, 2018.
- [38] Nathalie Japkowicz and Shaju Stephen. The class imbalance problem: A systematic study. *Intelligent Data Analysis*, 6(5):429–449, 2002.
- [39] Jonathon Byrd and Zachary Lipton. What is the effect of importance weighting in deep learning? In Kamalika Chaudhuri and Ruslan Salakhutdinov, editors, *Proceedings of the 36th International Conference on Machine Learning*, volume 97 of *Proceedings of Machine Learning Research*, pages 872–881. PMLR, 09–15 Jun 2019.
- [40] Thomas M. Cover and Joy A. Thomas. *Elements of Information Theory (2. ed.)*. Wiley, 2006.
- [41] Kaiming He, Xiangyu Zhang, Shaoqing Ren, and Jian Sun. Deep residual learning for image recognition. In *Proceedings of the IEEE Conference on Computer Vision and Pattern Recognition*, pages 770–778, 2016.